European Geothermal Congress 2013
Pisa, Italy, 3-7 June 2013

Characterizing Fracture Properties in Geothermal Reservoirs using Electrical Resistivity Measurements with Conductive Fluid Injection

Lilja Magnusdottir[1], Roland N. Horne[1]

[1] Department of Energy Resources Engineering, Stanford University, 367 Panama St., Stanford, CA 94305 U.S.A.

liljam@stanford.edu

Keywords: Fracture Connectivity, Tracer Tests, Electrical Resistivity, Inverse Analysis, Thermal Breakthrough

ABSTRACT

This paper discusses a method of characterizing fracture connectivity in geothermal reservoirs using conductive fluid injection and electrical resistivity measurements. A 'library' of discrete fractal fracture networks with different spatial fractal dimensions was generated. For each of the networks, the time history of electric potential difference between well pairs was calculated as a conductive fluid was injected into the reservoir. The conductive fluid travels along fracture paths from the injector towards the producers causing the electric potential difference to drop. The changes in electric potential are related to the connectivity of the fracture network. One of the fracture networks was used as a hypothetical geothermal reservoir and inverse modelling was used to match the time-history of the electric potential to other fracture networks. For comparison, inverse analysis was also used to match tracer return curves alone and the study showed that locations of connected areas were estimated better using the electric potential approach. Thermal return curves for the reservoir were calculated and the results showed promising possibilities for using electric potential measurements to predict thermal breakthrough.

1. INTRODUCTION

Fracture configuration is central to the performance of Enhanced Geothermal Systems (EGS), as well as to that of conventional reservoirs in fractured volcanic rocks. Interconnected fractures control mass and heat transport in the reservoir and if injected fluid reaches production wells before it is fully heated, unfavorable effects on energy production will result due to decreasing fluid enthalpies. Consequently, inappropriate placement of injection or production wells can lead to premature thermal breakthrough. Such premature thermal breakthroughs have occurred in numerous geothermal reservoirs, as described by Horne (1982), and observed in The Geysers (Beal et al., 1994). Thus, characterizing fractures in the reservoir is crucial to ensure adequate supply of geothermal fluids and efficient thermal operation of the wells.

Current geophysical methods, such as self-potential and direct current surveys are commonly used to explore geothermal fields (Garg et al., 2007). Seismic and electromagnetic surveys have also been useful for identifying boundaries between flow units (Chen, 2010; Parra et al., 2006) and to detect fractures at small depth (Jeannin, 2006). However, at greater depth these surveys cannot identify fractures that are small-scaled in comparison to the reservoir.

In the method considered in this study, conductive fluid injection would be used with electrical resistivity measurements to estimate the connectivity of fracture networks. The electric potential drops as conductive fluid fills fractures from the injector towards the producer. Therefore, the time-lapse electric potential data are related to the connectivity of the fracture network. Electrodes would be placed inside the geothermal wells to measure the resistivity more accurately in the deeper part of the reservoir. Irving and Singha (2010) have demonstrated an attempt to use Bayesian Markov-chain-Monte-Carlo (McMC) methodology to jointly invert dynamic cross-well and surface resistivity data with tracer concentration data to estimate hydraulic conductivities in heterogeneous geological environments. They concluded that using resistivity data instead of tracer data alone was worth the most where flow was controlled largely by highly connected flow paths. A key difference in our study is that we are estimating the connectivity of reservoirs with discrete fractures instead of grid-blocks.

Field studies by Rouleau and Gale (1985) suggest that fracture connectivity is dependent on fracture orientation, spacing, and trace length but connectivity has also been quantified by the size of a group of linked fractures, known as a 'cluster' (Stauffer, 1985). In this project, the connectivity is characterized by the Fractional Connected Area (FCA) which is the fraction of the total area that is connected by clusters of fractures, as described by Ghosh and Mitra (2009). Fractional Connected Area provides a good indicator of the overall fracture density and does not relate the cluster size to only the connectivity within the largest cluster as seen in other methods (Odling, 1997).

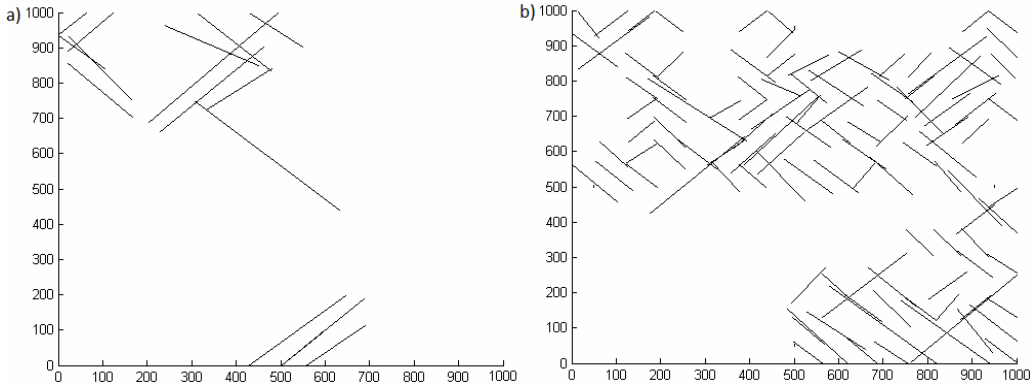

Figure 1: A fractal fracture network with fractal dimension equal to a) D = 1.0 and b) D = 1.8.

First, discrete fractal fracture networks were modelled representing fracture-dominated flow paths in geothermal reservoirs. Then, a flow simulator was used to simulate the flow of a conductive tracer through the networks and to solve the electric fields at each time step by utilizing the analogy between Ohm's law and Darcy's law. One of the networks was chosen as a hypothetical 'true' reservoir and inverse modelling was used to match the time-histories of the electric potential to other candidate fracture networks. This method was compared to estimating connectivity using tracer return curves alone. In the end, the possibility of using the electrical approach to estimate thermal-return curves was investigated.

2. A LIBRARY OF FRACTURE NETWORKS

A 'library' of discrete fractal fracture networks representing fractured geothermal reservoirs was generated. Time-histories of electric potential difference between well pairs were calculated for all the networks as a conductive fluid was injected into the reservoir. General Purpose Research Simulator (GPRS) developed at Stanford University (Cao, 2002) was used to simulate both the tracer flow and the electric fields at each time-step as demonstrated earlier by Magnusdottir and Horne (2012). This section describes how the fractal fracture networks were generated and modelled for the flow and electric simulations.

2.1 Discrete fractal fracture networks

Discrete fracture networks (DFN) were modelled using a Discrete Fracture Network (DFN) approach by Karimi-Fard et al. (2003) and the triangular mesh was formed using Triangle (Shewchuk, 1996). The fractures were assumed to follow a power-law length distribution as seen in field studies that have been performed on fault systems at different length scales (Shaw and Gartner, 1986; Main et al., 1990). The length distribution can be described by the following equations (Nakaya et al., 2003),

$$N(l) = Bl^{-a} \qquad [1]$$

$$a = \lim_{l \to 0} \log N(l) / \log(1/l) \qquad [2]$$

$$B = (l_{\max})^a \qquad [3]$$

where a is the fractal dimension of the fracture length distribution, l_{max} is the maximum fracture length and $N(l)$ is the number of fractures with lengths larger than l, so $l=l_{max}$ when $N(l)=1$. The spatial distribution of the fractures is also assumed to be fractal. Therefore, the relationship between the fractal dimension D within an $L \times L$ square domain and $N(r)$, the number of boxes of size r that include the center point of fractures, can be represented by a fractal equation using the box-counting approach (Barton and Larsen, 1985),

$$D = \lim_{r \to 0} \log N(r) / \log(1/r) \qquad [4]$$

where $r = L/k$ (k=1,2,3,…). Discrete-fracture networks with fractal dimensions ranging from D = 1.0 to 1.8 with 0.1 increments were created using a method described by Nakaya et al. (2003). The angles normal to the fractures were chosen to have two different distributions, both equally as likely to be chosen. The angles had a normal distribution with the mean either as 45° or as 135°, and with a standard deviation of 5°. The maximum fracture length was set as l_{max}=600 m and the aperture was defined by,

$$w_{\max} = C \cdot l^e \qquad [5]$$

where w_{max} is the aperture and C is a constant. Olson (2003) describes how this power law equation was used to fit various fracture datasets of different sizes, usually with e = 0.4. Here, e was set as 0.4, C as 0.002 $m^{3/5}$ and the size of the reservoir was set as 1000 × 1000 m^2. Figure 1 shows an example of a fracture network with fractal dimension D = 1.0 and one with D = 1.8. The fracture connectivity for the network with higher fractal dimension is considerably better.

2.2 Simulation using GPRS

The conductive tracer injected into the reservoirs was assumed to be a NaCl solution and the resistivity of the solution, ρ_w, was calculated using a three-dimensional regression formula established by Ucok et al. (1980). They concluded that the dependence of resistivity is best represented by the formula:

$$\rho_w = b_0 + b_1 T^{-1} + b_2 T + b_3 T^2 + b_4 T^3 \qquad [6]$$

where T is temperature and b are coefficients found empirically. The best fit for the concentration dependence was found to be:

$$\rho_w = 10/(\Lambda c) \quad [7]$$

$$\Lambda = B_0 - B_1 c^{1/2} + B_2 c \ln(c) + higher\ order\ terms \quad [8]$$

Coefficients B depend on the solution chemistry and c is the molar concentration.

In this project, the tracer concentration resulting from the flow simulation is changed into molar concentration and the following B coefficient matrix for the three-dimensional regression analysis of the data studied by Ucok et al. (1980) is used to calculate the resistivity of the NaCl solution,

$$B = \begin{matrix} 3.470 & -6.650 & 2.633 \\ -59.23 & 198.1 & 64.80 \\ 0.4551 & -0.2058 & 0.005799 \\ -0.346E\text{-}5 & 7.368E\text{-}5 & 6.741E\text{-}5 \\ -1.766E\text{-}6 & 8.787E\text{-}7 & -2.136E\text{-}7 \end{matrix}$$

Then, the resistivity of the water saturated rock, ρ, was calculated using Archie's law (Archie, 1942),

$$\rho = m\phi^{-n}\rho_w \quad [9]$$

where □ is the porosity of the rock, ρ_w is the resistivity of the NaCl solution and m and n are empirical constants. Archie (1942) concluded that for typical sandstones in oil reservoirs the coefficient m is approximately 1 and n is approximately 2 but Keller and Frischknecht (1996) showed that this power law is valid with varying coefficients based on the rock type. In this case, m was set as 0.62 and n as 1.95, which corresponds to well-cemented sedimentary rocks with porosity 5-25% (Keller and Frischknecht, 1996).

For the fracture network examples used in this study, one injection and three production wells were modelled. Water was injected at the rate of 10 kg/s and conductive tracer was 22 wt% of the water injected. The fractures were modeled to be filled with (fresh) water before any conductive tracer was injected so the initial tracer mass was set to 0.05 wt%. The production wells were modelled to deliver against a bottom-hole pressure of 10^6 Pa with productivity index of 4×10^{-12} m^3. The initial pressure was set to 10^6 Pa and the temperature to 25°C. The porosity of the fractures was defined as 0.9 and the permeability was determined by:

$$k = \frac{w^2}{12} \quad [10]$$

where w is the aperture of the fractures. The matrix blocks were given a porosity value of 0.1 and the permeability was set as 1×10^{-10} m^2. After using GPRS to solve for the tracer flow, the analogy between Darcy's law and Ohm's law (Muskat, 1932) was utilized and GPRS used to also solve the electric field. An electric current was set equal to 1 A at the injector and as -1 A at Producer 1 and the potential field was calculated based on the resistivity of the field at each time step. Then, the same procedure was repeated for all the other well pairs. Further details about how GPRS was used to calculate the electric field can be found in Magnusdottir and Horne (2012).

2.3 Number of fracture networks increased

The computer power available for this study allowed for 800 candidate fracture networks to be generated. In order to increase the number of distinctive fracture networks the mirror images of the networks were used as well. The location of the injector and producers is symmetrical about a vertical line in the middle of the reservoir. For a fracture network, the electric potential between the injector and Producer 1, is the same as the electric potential between injector and Producer 2 for the mirror image of the network (and vice versa) (Figure 2). The same applies for electric potential between Producer 1 and Producer 3, and between Producer 2 and Producer 3. Other well pairs are unchanged. Thus, the number of distinctive fracture networks was doubled and a total of 1600 different fracture networks were used for the inverse analysis in this study.

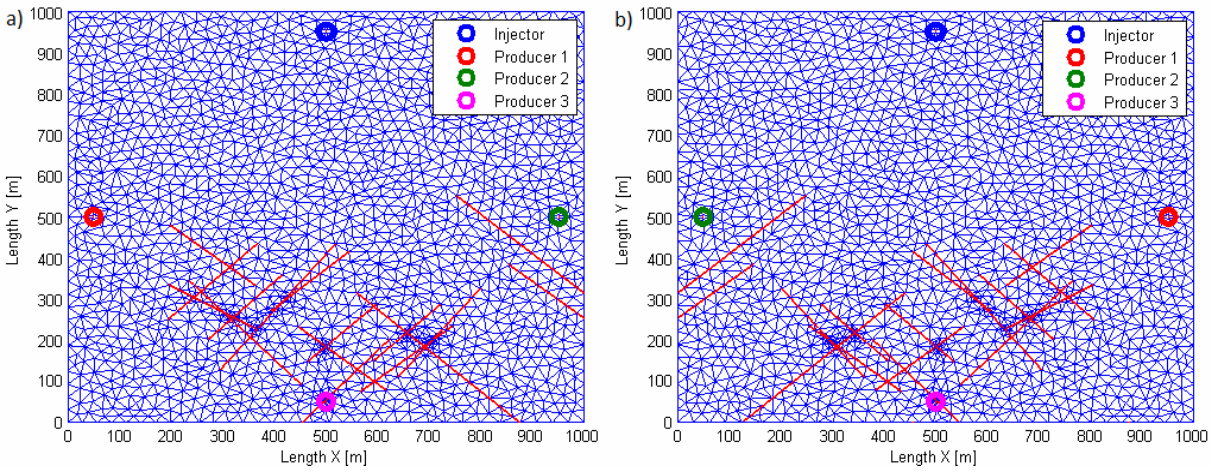

Figure 2: a) A fractal fracture network b) The mirror image of the fracture network in a).

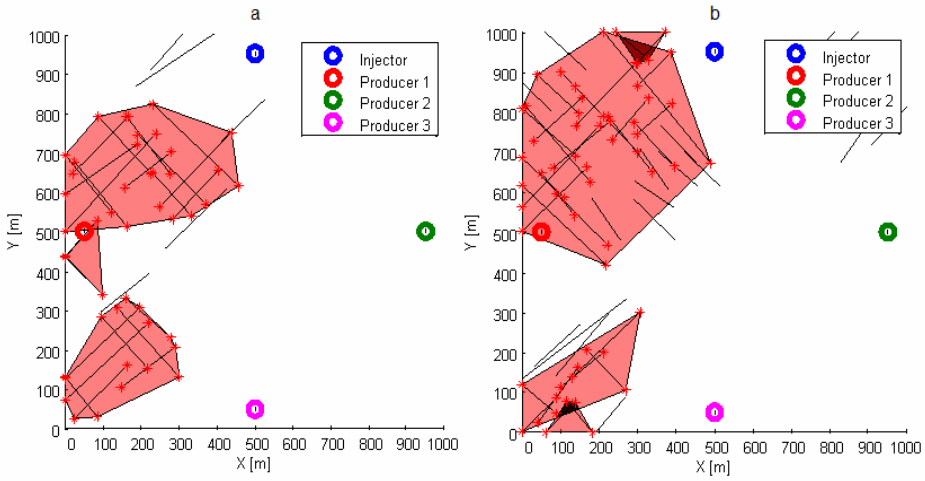

Figure 3: a) A hypothetical reservoir and b) the best match when using electric potential difference between wells.

3. INVERSE ANALYSIS

One of the fracture networks in the library of 1600 networks was chosen as a hypothetical 'true' geothermal reservoir. Inverse analysis was used with the time histories of the electric potential to estimate the connectivity of the reservoir. The connectivity was quantified by Fractional Connected Area (FCA). FCA is defined by the summed area of all clusters within a fracture network divided by the total sample area where the area of a cluster is delineated by the simplest polygon around the extremities of a fracture cluster.

Due to the relatively small number of fracture networks, a grid search algorithm could be used to compare the reservoir response to that of all the fracture networks in the library of networks. For the 'true' reservoir, the best match was found using least squares, where the sum of the squared deviations between the electric curves for the true reservoirs and the electric curves for the fracture networks is minimized. For every well pair in the reservoir, the following least squares criterion was calculated,

$$Q_j = \sum_{i=1}^{n} (y_i - f_i)^2 \qquad [11]$$

where y_i is the electric potential difference between well pair j in the true reservoir at time i and f_i is the corresponding electric potential for the fracture network. Then, the sum of Q_j for all well pairs was minimized to find the best match.

3.1 Hypothetical reservoir

The fracture network chosen as the 'true' geothermal reservoir is shown in Figure 3a. The spatial fractal dimension of the reservoir is D = 1.2 and the Fractional Connected Area (FCA) is 18%. Electric potential difference between well pairs and tracer return curves at the producers are shown in Figure 4. The electric potential difference between the injector and Producer 1 drops considerably faster than that between other well pairs due to the connected area between the injector and Producer 1. After the conductive tracer reaches Producer 1, the tracer travels towards Producer 3 through the fractured area in the lower left corner of the reservoir. The tracer travels, however, relatively slowly towards Producer 2 because there are no fractures in that area. The tracer return curves at the producers also indicate a considerably better connection towards Producer 1 than towards the other producers. The tracer reaches Producer 1 after 1 day but reaches Producer 2 after 26 days and Producer 3 after 28 days.

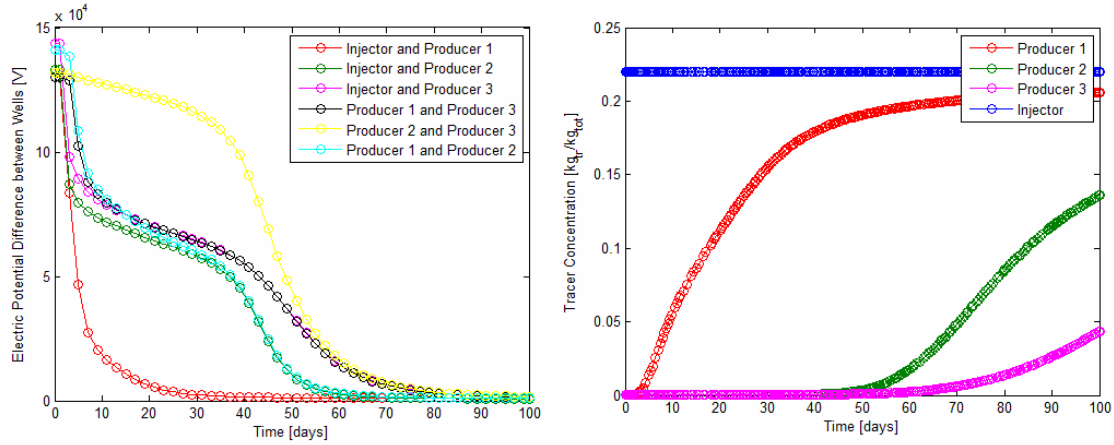

Figure 4: Electric potential difference between wells (to the left) and tracer return curves (to the right).

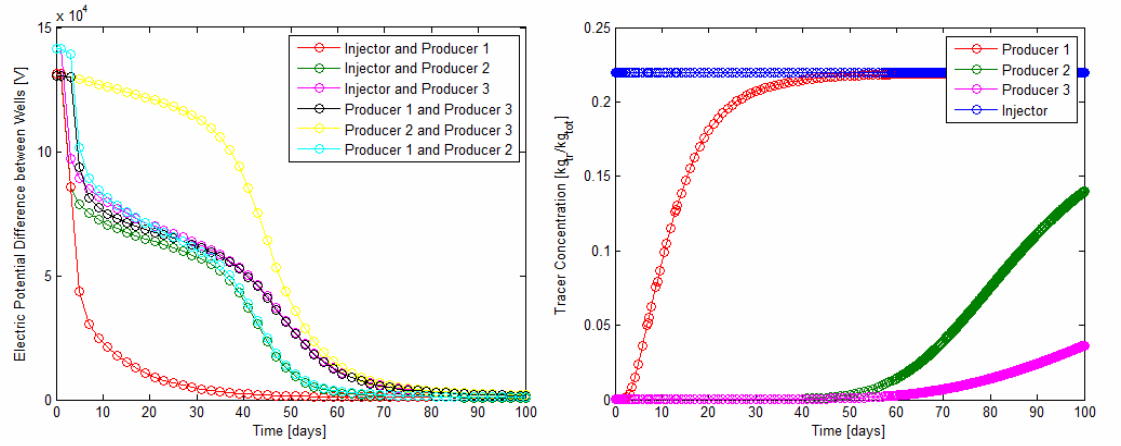

Figure 5: The electric potential difference between wells (to left) and tracer return curves (to right) for the fracture network in Figure 3b.

3.2 Inversion of electric potential data

The inverse analysis compared the time histories of the electric potential difference between well pairs for the reservoir in Figure 3 to the 'library' of 1600 fracture networks. The network that gave the best match is seen in Figure 3b. The curves for the electric potential (Figure 5) show a very similar behaviour to the curves for the true reservoir described previously in Figure 4.

The Fractional Connected Area (FCA) of the network in Figure 3b was compared to the FCA of the true reservoir. The results were FCA = 25% for the best match while FCA for the reservoir was FCA = 18%. Thus, FCA matches relatively well. The difference in FCA can be explained by fractures in the true reservoir that are located close to the injector and leading towards Producer 1, but do not intersect any of the fractures in the connected area. These few fractures contribute to the flow but do not increase the size of the connected area. In another case studied previously (Magnusdottir and Horne, 2013) FCA matched very well but this example demonstrates that large fractures not intersecting other fractures can also contribute significantly to the flow. Thus, estimating FCA with very high precision is not of interest here but to rather obtain an idea of where the fractures contributing to the flow are located in order to better understand the flow system.

The location of the connected areas is another similarity that can be seen between the best match and the real reservoir. In both cases the connected fractures are located similarly between the injector and Producer 1, resulting in a drop in potential difference between these wells as conductive fluid is injected into the reservoir. The connected area in the lower left corner of Figure 3a is also predicted correctly, causing the tracer to travel from the upper connected area, along the left side of the reservoir, towards Producer 3. Therefore, the electric potential difference between Producer 1 and Producer 3 drops considerably faster than the electric potential difference between Producer 2 and Producer 3. These results indicate a good possibility of using this electric approach to determine fractional connected area as well as the general locations of the connected fractures.

The tracer return curves for the best match, shown in Figure 5, show somewhat different behavior than the tracer return curves for the hypothetical reservoir (Figure 4). Thus, it was of interest to compare the performance results of using the electrical approach to those using only tracer return curves to predict connected areas.

3.3 Inversion of tracer return curves

The inverse analysis was performed again for the reservoir in Figure 3a, but this time the objective function measured the difference between the model calculation of just the simple tracer return curves and the corresponding tracer return curves for the true reservoir. The best match when comparing the tracer return curves can be seen in Figure 6. For this case, the time histories of the electric potential difference between the wells (Figure 7) do not match as well as when they were used to find the best match. However, as expected, the tracer return curves match better than before.

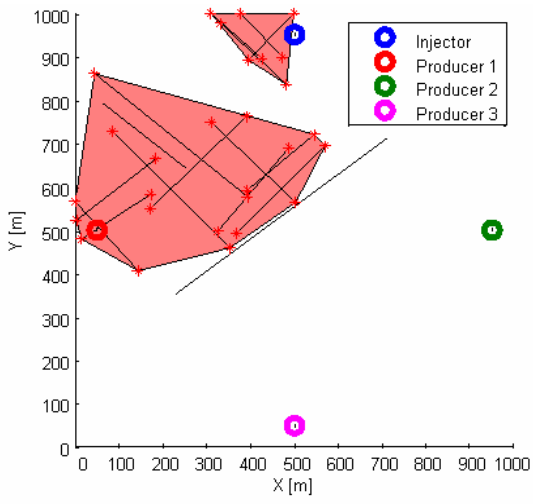

Figure 6: The best match when using tracer return curves.

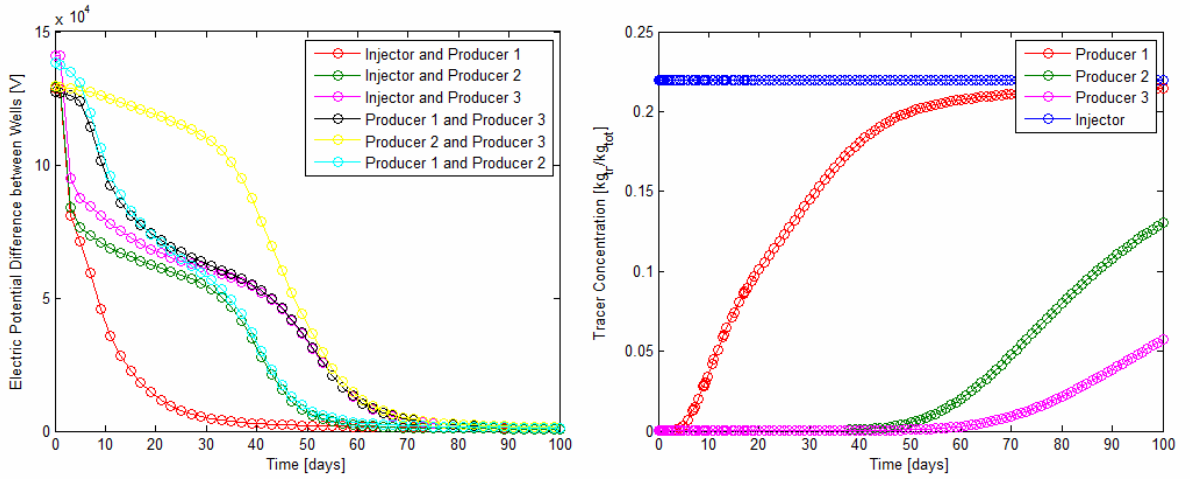

Figure 7: The electric potential difference between wells (to left) and tracer return curves (to right) for the fracture network in Figure 6.

Here, FCA = 19% so FCA matches very well to the true reservoir where FCA = 18%. However, for the best match all of that connected area is located only between the injector and Producer 1. Thus, tracer return curves indicate a good connection between the injector and Producer 3 but fail to predict the connected area between Producer 1 and Producer 3.

The location of connected area is better predicted using the electric approach and the same observation was also valid for other cases not shown here (another example is shown in Magnusdottir and Horne, 2013). The advantages of using the electric measurements include having more extensive data and being able to see the changes as the conductive fluid flows through the network even before the tracer would have reached the production wells.

4. ESTIMATION OF THERMAL RETURN

Thermal return curves were studied to investigate the possibility of using electrical potential measurements to predict temperature declines in geothermal reservoirs. The initial temperature of the reservoirs was set as 200°C and the injected fluid was at 100°C. Water was injected at 1 kg/s and the production wells were modelled to deliver against a bottom-hole pressure of 10^6 Pa with productivity index of 4×10^{-12} m^3. Other parameters were unchanged.

Figure 8 shows the thermal return curves for the 'true' reservoir in Figure 3a and the best match reservoir based on the electric potential approach (Figure 3b). The thermal return curves for the best match show similar behaviour to that of the 'true' reservoir. The temperature declines considerably faster in Producer 1 than in the other producers due to the connected area located between the injector and Producer 1. Therefore, the production rate in Producer 1 would need to be decreased to prevent premature thermal breakthrough.

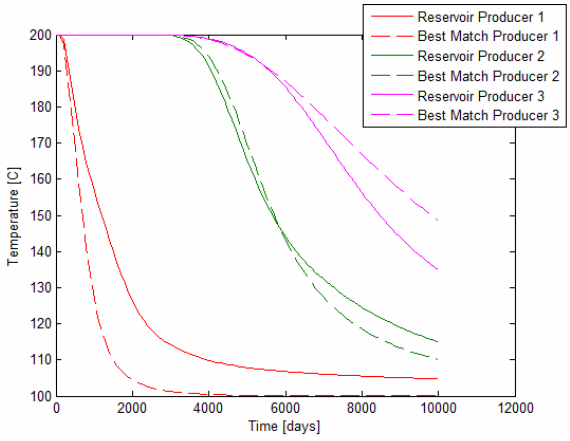

Figure 8: Thermal return curves for the true reservoir in Figure 3a and the best match using electric potential approach (Figure 3b).

Other cases were also studied, as shown in Figure 9. The thermal return curves in Figure 9c for the reservoir in Figure 9a show very similar behaviour to the best match (Figure 9b). The temperature at Producer 1 and at Producer 3 drops slowly because there are no fractures in the top half of the reservoir. Thus, there are no fast-flow paths leading towards these producers causing premature thermal breakthrough as seen previously in Figure 8. The reservoir in Figure 9d and the best match in Figure 9e have similar connected areas in the top part of the reservoirs, causing the temperature to drop relatively quickly at Producer 1 and Producer 2. However, the drop is not as steep as seen at Producer 1 in Figure 8. The behaviour at Producer 3 for this example is also similar for the reservoir and the best match.

These examples have shown promising possibilities for using inversion of electric potential measurements with conductive fluid injection to gain information about thermal return curves. Future work involves further investigating this potential and to compare this method to predicting thermal return curves using only tracer tests.

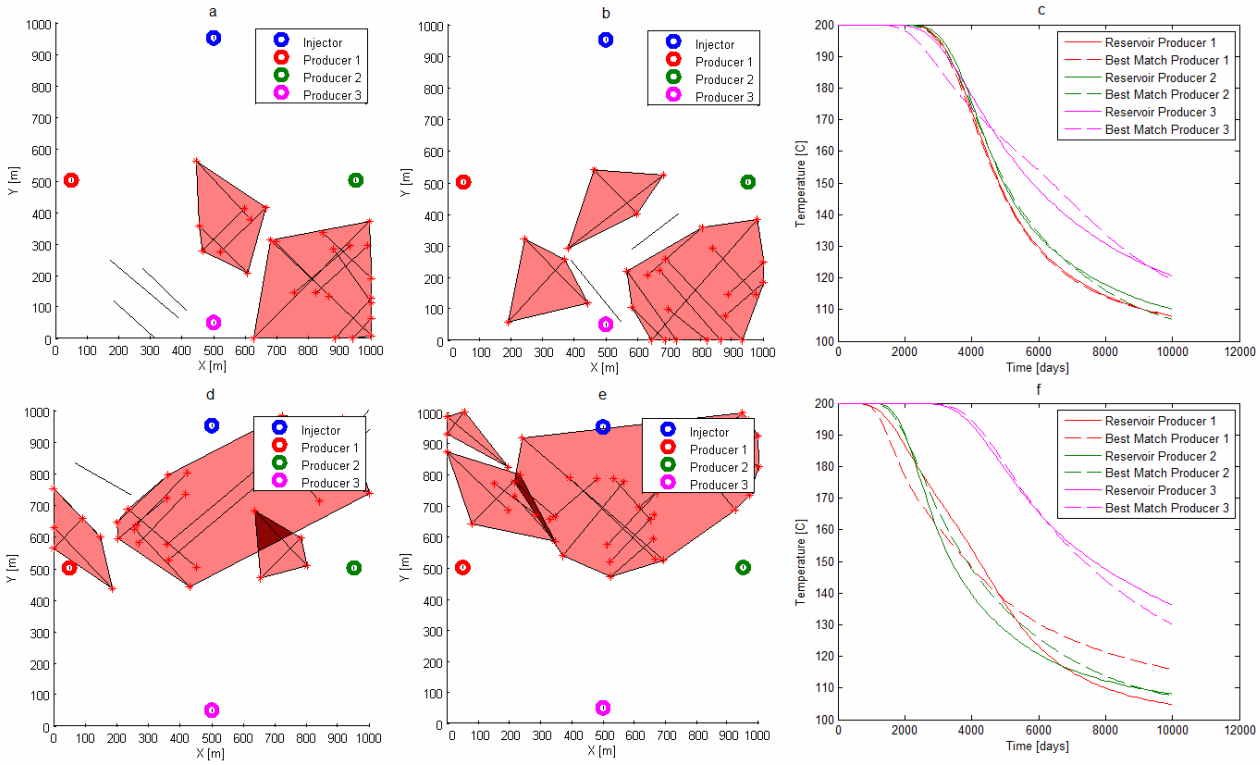

Figure 9: a) Reservoir 2, b) best match for Reservoir 2 when using electric potential, c) thermal return curves for Reservoir 2, d) Reservoir 3, e) best match for Reservoir 3 when using electric potential, f) thermal return curves for Reservoir 3.

5. CONCLUSIONS

In this work, time histories of electric potential difference between wells were used in an inverse analysis to estimate the Fractional Connected Area (FCA) of a hypothetical reservoir. A library of fracture networks was generated and the electric potential computed as a conductive fluid was injected into the reservoir. One of the networks was chosen as a hypothetical 'true' reservoir and the time-lapse electric potential data was compared to all the other networks to find the best match using a grid-search algorithm. The reservoir and the best match had a similar FCA and the connected areas had similar locations. For comparison, the inverse analysis was also performed matching only the tracer return curves at the producers. The best match gave similar FCA but the locations of the connected areas were somewhat different from those of the true reservoir. The same observation was made in other examples not included here.

The possibility of using the electric approach to estimate thermal breakthrough was investigated. Thermal return curves for the true reservoir and the best match obtained using the electric approach showed similar behaviour. Additionally, other cases studied also showed similar temperature decline for the chosen reservoirs and their best matches. Future work will include investigating this possibility further.

ACKNOWLEDGEMENT

This research was supported by the US Department of Energy, under Contract DE-FG36-08GO18192. The Stanford Geothermal Program is grateful for this support.

REFERENCES

Archie, G. E.: The Electrical Resistivity Log as an Aid in Determining some Reservoir Characteristics, *Transaction of the American Institute of Mining, Metallurgical and Petroleum Engineers*, **146**, (1942), 54-62.

Barton C., Larsen E.: Fractal geometry of two-dimensional fracture networks at Yucca Mountain, southwestern Nevada, *International Symposium on Fundamentals of Rock Joints*, Bjorkliden, Sweden, (1985).

Beal, J. J., Adams, M. C. and Hrtz, P. N.: R-13 Tracing of Injection in The Geysers, *Geothermal Resources Council*, **18**, (1994), 151-159.

Cao, H.: Development of Techniques for General Purpose Simulators, *PhD Thesis*, Stanford University, USA, (2002).

Chen, J., Hubbard S. S., Gaines D., Korneev V., Baker G., Watson D.: Stochastic estimation of aquifer geometry using seismic refraction data with borehole depth constraints, *Water Resour. Res.* 46:W11539, (2010). Doi:10.1029/ 2009WR008715.

Garg, S. K., Pritchett, J. W., Wannamaker, P. E. and Combs, J.: Caracterization of Geothermal Reservoirs with Electrical Surveys: Beowawe geothermal field, *Geothermics*, **36**, (2007), 487-517.

Ghosh, K. and Mitra, S.: Two-Dimensional Simulation of Controls of Fracture Parameters on Fracture Connectivity, *AAPG Bulletin*, **93**, (2009), 1517-1533. Doi: 10.1306/07270909041.

Horne, R. N.: Effects of Water Injection into Fractured Geothermal Reservoirs, a Summary of Experience Worldwide, *Geothermal Resources Council*, Davis, CA, **12**, (1982), 47–63.

Irving, J. and Singha K.: Stochastic inversion of tracer test and electrical geophysical data to estimate hydraulic conductivities, *Water Resour. Res.*, **46**, (2010). Doi:10.1029/2009WR008340.

Jeannin, M., Garambois S., Greégoire D., Jongmans D.: Multiconfiguration GPR measurements for geometric fracture characterization in limestone cliffs (Alps), *Geophysics*, **71**, (2006), B85-B92. Doi:10.1190/1.2194526.

Karimi-Fard, M., Durlofsky, L.J. and Aziz, K.: An Efficient Discrete Fracture Model Applicable for General Purpose Reservoir Simulators, SPE 79699, *SPE Reservoir Simulation Symposium*, Houston, TX, (2003).

Magnusdottir, L. and Horne, R. N.: TOUGH2 flow simulator used to simulate an electric field of a reservoir with a conductive tracer for Fracture characterization, *Geothermal Resources Council, 36th Annual Meeting and GEA Trade Show*, Reno, Nevada, (2012).

Magnusdottir L., Horne R. N.: Fracture Connectivity of Fractal Fracture Networks Estimated using Electrical Resistivity, *Proceedings, 38th Workshop on Geothermal Reservoir Engineering*, Stanford University, Stanford, CA, (2013).

Main, I. G., Meredith, P. G., Sammonds, P. R, and Jones, C.: Influence of fractal flaw distributions on rock deformation in the brittle field, in Deformation Mechanisms, Rheology and Tectonics, edited by Knipe, R.J. and Rutter, E. H., *Geol. Spec. Publ*., London, **54**, (1990), 71-79.

Muskat, M.: Potential Distributions in Large Cylindrical Disks with Partially Penetrating Electrodes, *Physics*, **2**, (1932), 329-364.

Nakaya, S., Yoshida, T. and Shioiri, N.: Perlocation Conditions in Binary Fractal Fracture Networks: Applications to Rock Fractures and Active and Seismogenic Faults, *J. Geophys. Res.*, **108**(B7), (2003), 2348. Doi: 10.1029/2002JB002117.

Odling, N. E.: Scaling and connectivity of joint systems in sandstones from western Norway, *Journal of Structural Geology*, **19**, (1997), 1251–1271.

Olson, J. E.: Sublinear scaling of fracture aperture versus length: an exception or the rule?, *Journal of Geophysical Research*, **108**, (2003), 2413. Doi:10.1029/2001JB000419.

Parra, J. O., Hackert, C. L., Bennett M. W.: Permeability and porosity images based on P-wave surface seismic data: Application to a south Florida aquifer, *Water Resour. Res.*, **42**, (2006). Doi:10.1029/2005WR004114.

Rouleau, A., and Gale, J. E.: Statistical characterization of the fracture system in the Stripa granite, *International Journal of Rock Mechanics and Mining Sciences and Geomechanics Abstracts*, Sweden, **22**, (1985), 353–367. Doi:10.1016/0148-9062 (85)90001-4.

Shewchuk, J. R.: Triangle: Engineering a 2D Quality ;Mesh Generator and Delaunay, (1996).

Stauffer, D.: Introduction to percolation theory, *Taylor and Francis*, London, **190,** (1985).

Ucok, H., Ershaghi, I. and Olhoeft, G. R.: Electrical Resistivity of Geothermal Brines, *Journal of Petroleum Technology*, **32**, (1980), 717-727.